Optical spectral weight distribution in d-wave superconductors

J.P. Carbotte[1] and E. Schachinger[2,*]

[1]*Department of Physics and Astronomy, McMaster University, Hamilton, Ontario, L8S 4M1 Canada*

[2]*Institute for Theoretical and Computational Physics, Graz University of Technology, A-8010 Graz, Austria*

(Dated: February 2, 2008)

The distribution in frequency of optical spectral weight remaining under the real part of the optical conductivity in the superconducting state of a d-wave superconductor depends on impurity concentration, on the strength of the impurity potential as well as on temperature and there is some residual absorption even at $T = 0$. In BCS theory the important weight is confined to the microwave region if the scattering is sufficiently weak. In an Eliashberg formulation substantial additional weight is to be found in the incoherent, boson assisted background which falls in the infrared and is not significantly depleted by the formation of the condensate, although it is shifted as a result of the opening of a superconducting gap.

PACS numbers: 74.20.Mn 74.25.Gz 74.72.-h

I. INTRODUCTION

When a metal enters its superconducting state, optical spectral weight is lost at finite frequencies under the real part of the optical conductivity, $\sigma_1(T,\omega)$.[1] Provided the change in kinetic energy between normal and superconducting state is small and can be neglected, the missing spectral weight reappears as a contribution at zero frequency which originates in the superfluid, and the over all optical sum rule of Ferrell, Glover, and Tinkham[2,3] remains unchanged. The distribution in frequency of the remaining spectral weight under $\sigma_1(\omega)$ ($\omega > 0$) depends on gap symmetry, on the nature of the inelastic scattering involved, on the concentration and scattering strength of the impurities, and on temperature.[4] In this paper we consider explicitely the case of d-wave gap symmetry within a generalized Eliashberg formalism.[5] In this approach the optical conductivity (as well as the quasiparticle spectral density) contains an incoherent part associated with boson assisted absorption which is not centered about zero frequency and which contributes to the optical spectral weight in the infrared range. In addition there is the usual quasiparticle contribution of BCS theory. Alternate approaches to include inelastic scattering exist. In several works, the quasiparticle scattering rate due to coupling to spin fluctuations is simply added to a BCS formalism through an additional scattering channel.[6,7,8,9] Nevertheless, whenever we refer to BCS within this paper we mean the standard theory without these additional features.

In BCS theory the London penetration depth[10,11] at zero temperature [$\lambda_L(0)$] in the clean limit is given by $\lambda_L^{-2}(0) = \lambda_{cl}^{-2}(0) = 4\pi ne^2/m = \Omega_p^2$ (n is the free electron density, e is the charge on the electron, m is its mass, Ω_p is the plasma frequency, and we have set the velocity of light equal to 1) and all the optical spectral weight condenses. However, as the impurity mean free path is reduced, not all the spectral weight is transferred to the condensate[12,13] and there remains some residual impurity induced absorption.[14,15,16] Details depend on gap symmetry.

In Eliashberg theory the pairing interaction is described by an electron-phonon spectral density, denoted by $\alpha^2F(\omega)$.[10,11,17] Twice the first inverse moment of $\alpha^2F(\omega)$, gives the quasiparticle mass renormalization with the effective (m^*) to bare (m) mass ratio $m^*/m = 1 + \lambda$. While the gap and renormalization function of Eliashberg theory acquire a frequency dependence which requires numerical treatment, a useful, although not exact, approximation is to assume that the important frequencies in $\alpha^2F(\omega)$ are much higher than the superconducting energy scale and, thus, one can approximate the renormalizations by a constant λ value.[11] In this approximation, the zero temperature penetration depth is $\lambda_L^{-2}(0) \simeq (4\pi ne^2/mc^2)[1/(1+\lambda)]$ in the clean limit. Thus, the electron-phonon renormalization simply changes the bare mass in the London expression to the renormalized mass m^*. This result does not depend explicitly on the gap and holds independent of its symmetry. A naive interpretation of this result is that only the coherent quasiparticle part of the electron-spectral density [which contains approximately $1/(1+\lambda)$ of the total spectral weight of one] condenses. While this is approximately true, we will see that the incoherent part which contains the remaining $\lambda/(1+\lambda)$ part of the spectral weight is also involved, although in a more minor and subtle way.

In an s-wave superconductor the entire incoherent part of the conductivity is shifted upward by twice the gap value, Δ, when compared to its normal state. It is also slightly distorted but, to a good approximation, it remains unchanged. The fact that there is a 2Δ shift between normal and superconducting state implies that an optical spectral weight shift originates from this contribution even if its overall contribution to the sum rule should remain the same. For a d-wave superconductor the situation is more complex because the gap is anisotropic and, thus, the shift by $2\Delta(\phi)$ varies with the polar angle ϕ on

the two-dimensional Fermi surface of the CuO_2 planes.

The goal of this paper is to understand, within an Eliashberg formalism, how the remaining area under the real part of the optical conductivity is distributed in frequency, how this distribution is changed by finite temperature effects and by the introduction of elastic impurity scattering, and what information can be obtained from such studies about the superconducting state and the nature of the mechanism which drives it.

In reference to d-wave superconductivity in the cuprates two boson exchange models which have received much attention are the Nearly Antiferromagnetic Fermi Liquid (NAFFL) model[18,19,20,21,22,23] and the Marginal Fermi Liquid (MFL) model.[24,25,26] Both models are characterized by an appropriate charge carrier-exchange boson spectral density $I^2\chi(\omega)$ which replaces the $\alpha^2F(\omega)$ of the phonon case[10,27,28,29] and which reflects the nature of the inelastic scattering envisioned. In the NAFFL model a further complication arises in that we would expect $I^2\chi(\omega)$ to be very anisotropic as a function of momentum on the Fermi surface. For simplicity we ignore this complication here. Also, in principle, a different spectral weight function can enter the gap and renormalization channel, respectively.

In Section II, we provide some theoretical background. The quasiparticle spectral density as a function of energy is considered as is the effect of impurities on it. In Sec. III we give the necessary formulas for the optical conductivity and discuss some results. In Sec. IV the conditions under which a partial sum rule involving only the quasiparticle part of the spectral density can be expected are described. Section V deals with issues associated with the residual absorption and Sec. VI deals with a more detailed discussion of optical spectral weight readjustment due to superconductivity. Conclusions are found in Sec. VII.

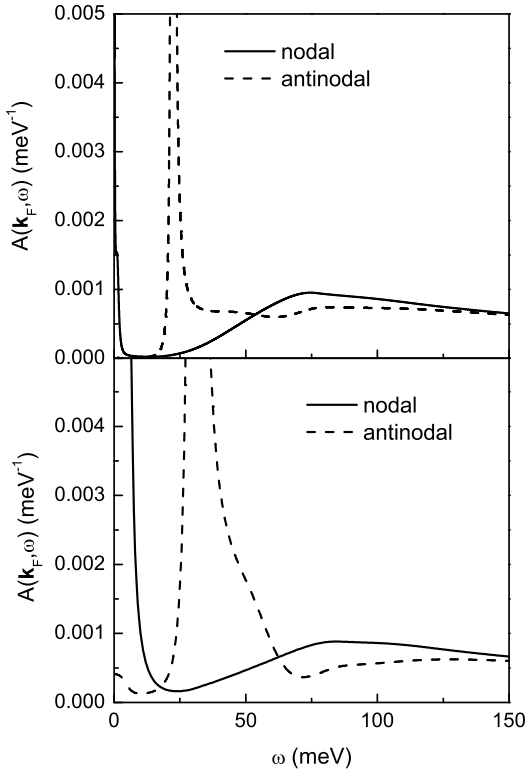

FIG. 1: The charge carrier spectral density $A(\mathbf{k}_F,\omega)$ as a function of ω for a d-wave superconductor based on the electron-spin fluctuation spectral density $I^2\chi(\omega)$ shown in the inset of Fig. 2. The solid curve applies to the nodal while the dashed curve is for the antinodal direction. The top frame is for a pure sample with impurity parameters $\Gamma^+ = 0.003\,\mathrm{meV}$ and $c = 0.2$ while the bottom frame is for $\Gamma^+ = 0.63\,\mathrm{meV}$ and $c = 0$.

II. QUASIPARTICLE SPECTRAL DENSITY

We begin with a discussion of the quasiparticle spectral density which will allow us to understand the basic features expected of the optical conductivity. In Nambu notation the 2×2-matrix Green's function $\hat{G}(\mathbf{k},\omega)$ in the superconducting state is given in terms of the single quasiparticle dispersion $\varepsilon_{\mathbf{k}}$ with momentum $\mathbf{k}$, the renormalized Matsubara frequency $\tilde{\omega}(\omega)$ and the pairing energy $\tilde{\Delta}_{\mathbf{k}}(\omega)$ which for a d-wave superconductor is proportional to $\cos(2\phi)$. In terms of Pauli's $\hat{\tau}$ matrices

$$\hat{G}(\mathbf{k},\omega) = \frac{\tilde{\omega}(\omega)\hat{\tau}_0 + \varepsilon_{\mathbf{k}}\hat{\tau}_3 + \tilde{\Delta}_{\mathbf{k}}(\omega)\hat{\tau}_1}{\tilde{\omega}^2(\omega) - \varepsilon_{\mathbf{k}}^2 - \tilde{\Delta}_{\mathbf{k}}^2(\omega)}. \qquad (1)$$

The quasiparticle spectral density $A(\mathbf{k},\omega)$ is given by

$$\begin{aligned} A(\mathbf{k},\omega) &= -\frac{1}{\pi}\Im\mathrm{m}G_{11}(\mathbf{k},\omega+i0^+) \\ &= -\frac{1}{\pi}\Im\mathrm{m}\frac{\tilde{\omega}(\omega+i0^+)+\varepsilon_{\mathbf{k}}}{\tilde{\omega}^2(\omega+i0^+)-\varepsilon_{\mathbf{k}}^2-\tilde{\Delta}_{\mathbf{k}}^2(\omega+i0^+)} \qquad (2) \end{aligned}$$

The generalized Eliashberg equations applicable to d-wave gap symmetry which include renormalization effects in the ω-channel have been written down before and will not be repeated here.[5] They are a set of coupled nonlinear integral equations for $\tilde{\omega}(\omega)$ and $\tilde{\Delta}_{\mathbf{k}}(\omega)$ which depend on an electron-boson spectral density $I^2\chi(\omega)$. The boson exchange mechanism involved in superconductivity is what determines its shape in frequency and its magnitude. In general, the projection of the electron-boson interaction on the $\tilde{\Delta}$ and $\tilde{\omega}$-channel can be different but for simplicity, here, the same form of $I^2\chi(\omega)$ is used in both channels but with a different magnitude: we use $gI^2\chi(\omega)$ with $g \neq 1$ for the $\tilde{\Delta}$-channel.

In Fig. 1 we present numerical results for $A(\mathbf{k}_F,\omega)$ based on numerical solutions of the Eliashberg equations. The kernel $I^2\chi(\omega)$ used for the numerical work is shown in the inset in the top frame of Fig. 2 and was obtained from consideration of the infrared optical conductivity of $YBa_2Cu_3O_{6.95}$ ($YBCO_{6.95}$).[22] Besides coupling to an optical resonance at 41 meV (the energy where a spin res-

onance is also seen in the inelastic neutron scattering[30]) which grows with decreasing temperature into the superconducting state, there is also additional coupling to a broad spin fluctuation spectrum background of the form introduced by Millis *et al.*[18] in their NAFFL model. This is seen as the long tail in $I^2\chi(\omega)$ which extends to very high energies of order 400 meV. The existence of these tails is a universal property of the cuprates.[12,13,23,31,32,33] This energy scale is of the order of the magnetic parameter J in the $t-J$ model.[34] A flat background spectrum is also characteristic of the MFL model.[24,25,26] In this work, the shape and size of $I^2\chi(\omega)$ is fixed from our previous fit to optical data[22] and left unchanged. It applies at low temperatures in the superconducting state ($T \sim 10$ K).

The top frame of Fig. 1 gives results for the charge carrier spectral density $A(\mathbf{k}_F, \omega)$ vs ω where $\mathbf{k}_F$ implies that we consider only the Fermi energy in Eq. (2). The results are for a pure sample with $\Gamma^+ = 0.003$ meV and $c = 0.2$. Here, Γ^+ is proportional to the impurity concentration and is related to the normal state impurity scattering rate (τ_{imp}^{-1}) equal to $2\pi\Gamma^+[1/(c^2+1)]$, where $c = 1/[2\pi N(0)V_{\rm imp}]$. $N(0)$ is the normal state density of states at the Fermi energy and $V_{\rm imp}$ the strength of the impurity potential. These impurity parameters were determined to fit well the microwave data in $YBCO_{6.99}$ obtained by Hosseini *et al.*[35] The solid curve is for the nodal direction and the dashed curve for the antinodal direction. The spectral gap is the value of $\Delta(\omega + i0^+) = \tilde{\Delta}(\omega + i0^+)/\tilde{\omega}(\omega + i0^+)$ evaluated at the frequency of the coherence peak in the density of states

$$\frac{N(\omega)}{N(0)} = \Re{\rm e}\left\langle \frac{\tilde{\omega}(\omega+i0^+)}{\sqrt{\tilde{\omega}^2(\omega+i0^+)-\tilde{\Delta}^2(\omega+i0^+)}}\right\rangle' \equiv \Re{\rm e}\left[\Omega(\omega)\right], \quad (3)$$

and is equal to 22.3 meV. This is also the position of the large peak seen in the dashed curve in the top frame of Fig. 1. However, there is no gap in the nodal direction, and in this case the spectral function is peaked about $\omega = 0$. It rapidly decays to nearly zero within a very narrow frequency range determined by a combination of the small impurity scattering rate which we have included and the equally small inelastic scattering which reflects the presence of $I^2\chi(\omega)$ and finite temperature. A second peak is also observed at higher energies but with reduced amplitude. This peak has its origin in the incoherent boson assisted processes described by the spectral density $I^2\chi(\omega)$. Note that the two contributions are well separated. In the constant λ model, the coherent part

$$A(\mathbf{k}_F,\omega) = \frac{1}{1+\lambda}\,\frac{\pi\Gamma^+/[(1+\lambda)(1+c^2)]}{\omega^2+\{\pi\Gamma^+/[(1+\lambda)(1+c^2)]\}^2}, \quad (4)$$

is a Lorentzian of width $\pi\Gamma^+/[(1+\lambda)(1+c^2)]$ and has total weight of $1/(1+\lambda)$. The remaining weight in the complete spectral density which is normalized to one, is thus to be found in the incoherent, boson assisted background. Returning to the antinodal direction, we see that in this case the separation between quasiparticle peak and incoherent boson assisted background is lost as the two contributions overlap significantly. In the bottom frame of Fig. 1 we show similar results for the charge carrier spectral density but now a larger amount of impurity scattering is included with $\Gamma^+ = 0.63$ meV (Ref. 36) and the unitary limit is taken, i.e. $c = 0$. In this instance, even for the nodal direction, impurities have the effect of filling in the region between quasiparticle and incoherent background (solid curve). Also for the antinodal direction (dashed curve), because we are in d-wave, the region below the gap energy which is now ~ 30 meV is filled in significantly. It would be zero in BCS s-wave. At $\omega = 0$, $\tilde{\omega}(0) = i\gamma$ and in antinodal direction

$$A(\mathbf{k}_F,\omega=0) = \frac{1}{\pi(1+\lambda)}\,\frac{\gamma/(1+\lambda)}{\Delta^2+[\gamma/(1+\lambda)]^2}, \quad (5)$$

which is finite. Here γ is the quasiparticle scattering rate at zero frequency in the superconducting state. It is calculated in Sec. V. This limit is not universal in contrast to the universal limit found by Lee[37] for the real part of the electrical conductivity at zero temperature which is $(ne^2/m)\{1/[\pi\Delta(1+\lambda)]\}$ in the constant λ model. Note that what enters the universal limit is the renormalized mass $m(1+\lambda) = m^*$ rather than the bare mass. This important fact has generally been overlooked in the discussion of this limit even though the difference can be numerically large (order ~ 3). We note one technical point about our Eliashberg numerical solutions. In all cases $I^2\chi(\omega)$ is kept fixed as is $T_c = 92$ K. In a d-wave superconductor the introduction of impurities, of course, reduces the critical temperature. What is done is that the parameter g which multiplies $I^2\chi(\omega)$ in the gap channel is readjusted slightly to keep T_c fixed. This procedure leads to the larger value of the spectral gap seen in the bottom frame of Fig. 1 as compared with the top frame (dashed lines).

III. INFRARED CONDUCTIVITY

A general expression for the infrared optical conductivity at temperature T in a BCS d-wave superconductor is[36,38,39]

$$\sigma(T,\nu) = -\frac{\Omega_p^2}{4\pi}\left\langle\left[-\int_0^\infty d\omega\,\tanh\left(\frac{\beta\omega}{2}\right)J(\omega,\nu)+\int_{-\nu}^\infty d\omega\,\tanh\left(\beta\frac{\omega+\nu}{2}\right)J(-\omega-\nu,\nu)\right]\right\rangle, \tag{6}$$

where the function $J(\omega,\nu)$ takes on the form

$$\begin{aligned} 2J(\omega,\nu) &= \frac{1}{E_1(\omega)+E_2(\omega,\nu)}\left[1-N(\omega)N(\omega+\nu)-P(\omega)P(\omega+\nu)\right] \\ &\quad+\frac{1}{E_1^*(\omega)-E_2(\omega,\nu)}\left[1+N^*(\omega)N(\omega+\nu)+P^*(\omega)P(\omega+\nu)\right]. \end{aligned} \tag{7}$$

In Eq. (6) $\beta = 1/k_BT$, with k_B the Boltzmann factor. In Eq. (7)

$$E_1(\omega) = \sqrt{\tilde{\omega}^2(\omega+i0^+)-\tilde{\Delta}^2(\omega+i0^+)}, \qquad E_2(\omega,\nu) = E_1(\omega+\nu), \tag{8a}$$

and

$$N(\omega) = \frac{\tilde{\omega}(\omega+i0^+)}{E_1(\omega)}, \qquad P(\omega) = \frac{\tilde{\Delta}(\omega+i0^+)}{E_1(\omega)}, \tag{8b}$$

and $E_1^*(\omega)$, $N^*(\omega)$, and $P^*(\omega)$ are the complex conjugates of $E_1(\omega)$, $N(\omega)$, and $P(\omega)$, respectively. These expressions hold for an Eliashberg superconductor as well as for BCS in which case the gap $\tilde{\Delta}(\omega)$ does not depend on frequency; it only depends on temperature, and on angle. Here, for brevity we have suppressed these dependencies but they are implicitly implied by the brackets $\langle\cdots\rangle$ in Eq. (6) which denote an angular average over momentum directions of electrons on the Fermi surface at a given temperature.

Figure 2 presents two fits of theoretical results to experimental data for the real part of the optical conductivity $\sigma_1(T,\omega)$. The top frame presents a comparison with data reported by Homes *et al.*[32] for an untwinned, optimally doped $YBCO_{6.95}$ single crystal (solid line) at $T = 10\,\mathrm{K}$. The dashed line corresponds to the best fit theoretical results generated using extended Eliashberg theory. The phenomenologically determined electron-boson spectrum $I^2\chi(\omega)$ reported by Schachinger *et al.*[22] (shown in the inset) was used. The impurity parameters $\Gamma^+ = 0.63\,\mathrm{meV}$ and $c = 0$ resulted in this best fit.[36] For comparison the dotted line corresponds to the results of a BCS calculation using the same impurity parameters. It is obvious that the BCS calculation cannot reproduce the boson assisted higher energy incoherent background which starts at about 80 meV. The full Eliashberg theory, on the other hand, is capable of modeling very well the experimental $\sigma_1(T,\omega)$ data over the whole infrared region. The bottom frame of Fig. 2 shows $\sigma_1(T,\omega)$ restricted to the microwave region up to $\omega = 0.1\,\mathrm{meV}$. Three temperatures are considered, namely $T = 10\,\mathrm{K}$ (solid curve), $T = 15\,\mathrm{K}$ (dashed curve), and $T = 20\,\mathrm{K}$ (dotted curve). The impurity parameters were varied to get a good fit to the data of a high purity $YBCO_{6.99}$ sample reported by Hosseini *et al.*[35] and presented by symbols. The best fit was found for $\Gamma^+ = 0.003\,\mathrm{meV}$ and $c = 0.2$. It is clear that this sample is very pure and that it is not in the unitary limit. All curves for $\sigma_1(T,\omega)$ vs ω in this frame show the upward curvature characteristic of finite c values. Unitary scattering would give a downward curvature in disagreement with the data.

The excellent agreement between theory and experiment shown in Fig. 2 encourages us to apply theory to discuss in detail, issues connected with the redistribution of optical spectral weight in going from the normal (not always available in experiment) to the superconducting state and the effect of temperature and impurities on it.

The real part of the optical conductivity $\sigma_1(T,\omega)$ as a function of ω is shown in the top frame of Fig. 3. A factor $\Omega_p^2/(8\pi)$ has been omitted from all theoretical calculations and so $\sigma_1(T,\omega)$ is in meV^{-1}. In these units the usual FGT sum rule which gives the total available optical spectral weight $\int_0^\infty d\omega\,\sigma_1(\omega) = \pi$ (including the superfluid contribution at $\omega = 0$). Two cases are shown in the frequency range $0^+ \le \omega \le 250\,\mathrm{meV}$. One is for the very pure sample (solid curve) with $\Gamma^+ = 0.003\,\mathrm{meV}$ and $c = 0.2$. The other is for a less pure sample (dotted curve) with $\Gamma^+ = 0.63\,\mathrm{meV}$ in the unitary limit, $c = 0$. In the solid curve we clearly see a separate quasiparticle contribution peaked about $\omega = 0$ which is responsible for a coherent Drude like contribution to the real part of the optical conductivity. In this process the energy of the photon is transferred to the electrons with the impurities providing a momentum sink. The width of the quasiparticle peak and corresponding Drude peak is related to the impurity scattering rate. Because we are using Eliashberg theory there is also a small contribution to this width coming from the thermal population

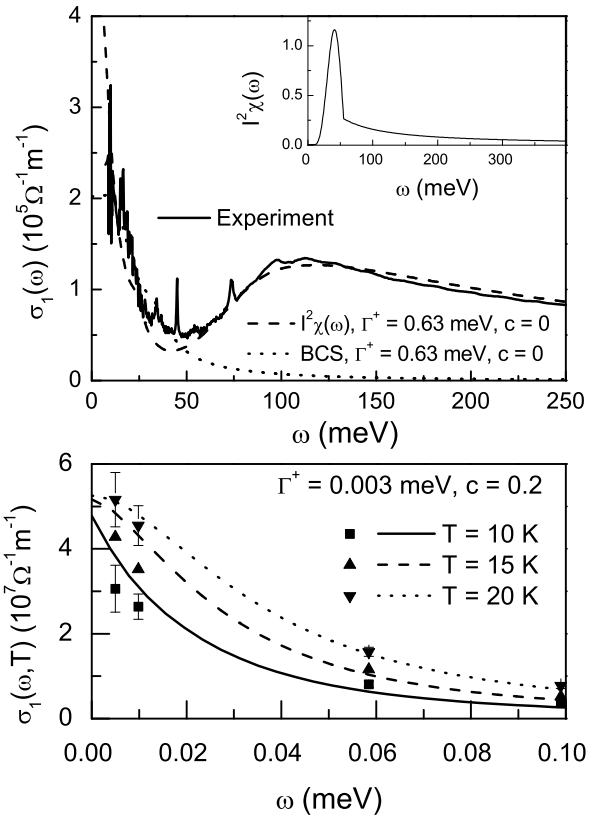

FIG. 2: Top frame: Real part of the optical conductivity $\sigma_1(T,\omega)$ vs ω for an optimally doped, untwinned $YBCO_{6.95}$ single crystal at $T = 10\,\mathrm{K}$. The solid line represents the experimental data reported by Homes *et al.*[32], the dashed line the result of a fit to a full Eliashberg calculation using the electron-boson spectral density $I^2\chi(\omega)$ shown in the inset and the impurity parameters $\Gamma^+ = 0.63\,\mathrm{meV}$ and $c = 0$.[36] The dotted line presents, for comparison, the result of a BCS calculation using the same impurity parameters. Bottom frame: the microwave region of $\sigma_1(T,\omega)$ for $\Gamma^+ = 0.003\,\mathrm{meV}$ and $c = 0.2$ which fits well the data of Hosseini *et al.*[35] (shown as symbols) for three temperatures, $T = 10\,\mathrm{K}$ (solid line), $T = 15\,\mathrm{K}$ (dashed line), and $T = 20\,\mathrm{K}$ (dotted line).[38] Again, the $I^2\chi(\omega)$ shown in the inset of the top frame has been used.

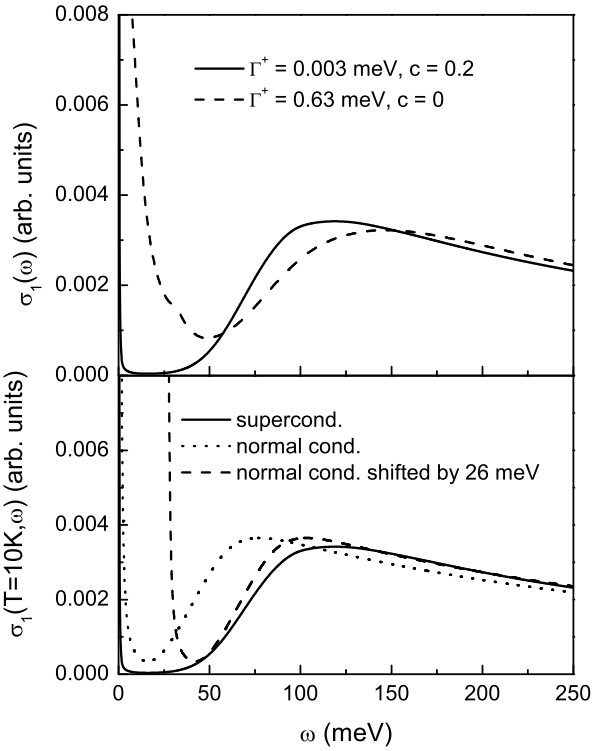

FIG. 3: Top frame: Real part of the optical conductivity $\sigma_1(\omega)$ vs ω in units of $\Omega_p^2/(8\pi)$. The solid curve is for a pure sample with impurity parameters $\Gamma^+ = 0.003\,\mathrm{meV}$, $c = 0.2$ and the dashed curve is for $\Gamma^+ = 0.63\,\mathrm{meV}$ and $c = 0$. The temperature $T = 10\,\mathrm{K}$. The electron-boson spectral density $I^2\chi(\omega)$ used is shown in the inset of the top frame of Fig. 2. For the solid curve, the narrow coherent quasiparticle peak centered at $\omega = 0$ is well separated from the higher energy incoherent, boson-assisted region. This separation is less clear in the dashed curve. Bottom frame: Real part of the optical conductivity $\sigma_1(T,\omega)$ vs ω in units of $\Omega_p^2/(8\pi)$ for a pure sample with impurity parameters $\Gamma^+ = 0.003\,\mathrm{meV}$ and $c = 0.2$ at $10\,\mathrm{K}$. The superconducting state (solid line) is compared with the normal state, i.e. setting the gap $\tilde{\Delta}(\omega) = 0$ in the Eliashberg equations (dotted line). The dashed curve is a repeat of the normal state curve but has been shifted in frequency by $26\,\mathrm{meV}$.

of excited spin fluctuations. In addition, there is a separate incoherent contribution at higher frequencies. This second contribution involves the creation of spin fluctuations during the absorption process. Its shape reflects details of the frequency dependence of the spectral density $I^2\chi(\omega)$ involved. For the normal state at temperature $T > T_c$ the spectral density $I^2\chi(\omega)$ in the NAFFL model does not show the resonance peak seen in the insert of the top frame of Fig. 2 but consists mainly of the reasonably flat background. This implies that in this region MFL behavior results with optical and quasiparticle lifetimes linear in frequency and in temperature. The energy scale associated with this behavior is the spin fluctuation scale ω_{SF}. This is verified in numerous experiments in the cuprates as reviewed by Puchkov *et al.*[31] Just as for the charge carrier spectral density discussed in the previous section, the optical weight under the coherent part, to which we add the superfluid contribution at $\omega = 0$, is about $1/(1+\lambda)$ of the total weight available ($\Omega_p^2/8$) with the remainder, $\lambda/(1+\lambda)$, to be found in the incoherent part. In the model considered here, which fits the available data for $YBCO_{6.99}$ and $YBCO_{6.95}$, $\lambda = 2.01$ so that only one third of the weight is in the coherent part. This order of magnitude agrees well with the extensive exper-

imental results in other cuprates given in Refs. 12,13. Note that coherent and incoherent region are nicely separated over a substantial frequency range in which the conductivity is small relative to its value in the quasiparticle peak and in the boson assisted background. This will lead to a plateau in the integrated optical spectral weight as a function of the upper limit ω in the integral over $\sigma_1(T,\omega)$ which will in turn lead to an approximate partial or truncated sum rule on the coherent contribution to the conductivity itself. It is only this piece which is included in BCS theory and which can be described by such a theory in cases when it is well separated from the incoherent background. We note that the addition of impurities, as in the dashed curve in the top frame of Fig. 3, greatly increases the frequency width of the quasiparticle peak in $\sigma_1(T,\omega)$ and also fills in the region between coherent and incoherent part of the conductivity. While these two contributions are still recognizable as distinct, they now overlap significantly and cannot as easily be separated.

Finally, but very importantly, in the bottom frame of Fig. 3 we repeat the curve for $\sigma_1(T,\omega)$ vs ω for the pure sample of the top frame of Fig. 3 (solid curve) and compare it with its normal state counterpart (dotted curve). We see that due to superconductivity, much of the weight under the Drude peak in the solid curve (superconducting) as compared with the dotted curve (normal) has been transferred to the condensate and is not part of the figure [δ-function at $\omega = 0$ in $\sigma_1(\omega,T)$]. It has also shifted the incoherent part to higher energies. For an s-wave superconductor the appropriate shift would be twice the gap as seen in the work of Marsiglio and Carbotte[1] (see their Fig. 11). For the d-wave case there is a distribution of gap values around the Fermi surface and consequently of upward shifts. This leads to some distortion of the incoherent part as compared with its normal state value as can be seen in the dashed curve which is the dotted curve displaced upwards by 26 meV, a value slightly larger than the gap of 22.3 meV and much less than twice the spectral gap. The difference between dashed and solid curve is small but not negligible. This shows that in the optical spectral weight distribution the boson assisted part of the spectrum is in a first approximation shifted in energy but not significantly depleted or augmented. The addition of impurities also have an effect on the incoherent background as can be seen in the top frame of Fig. 3 on comparison of the solid with the dashed curve.

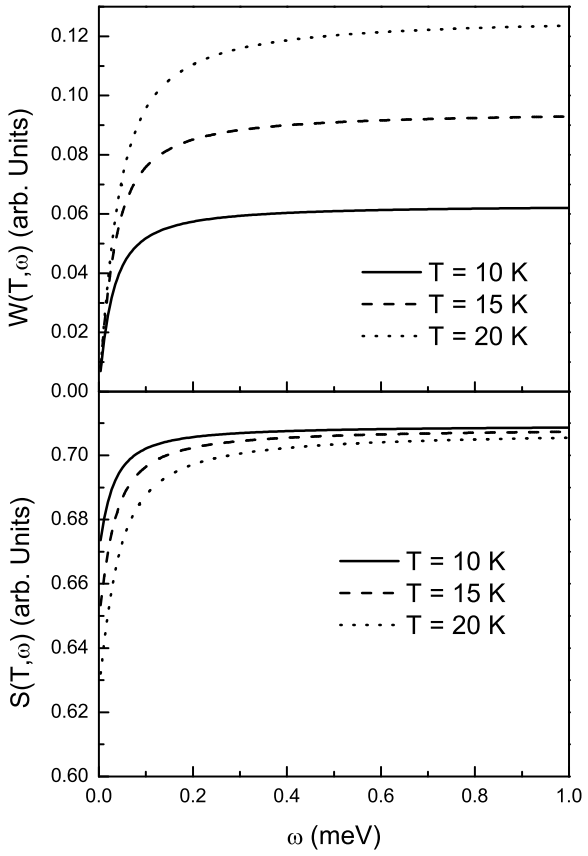

FIG. 4: The remaining integrated optical spectral weight in the superconducting state. Top frame: $W(T,\omega) = \int_{0^+}^{\omega} d\nu\, \sigma_1(T,\nu)$ for values of ω up to 1 meV. The temperatures are 10 K (solid lines), 15 K (dashed lines), and 20 K (dotted line). The gap is 22.3 meV, $\Gamma^+ = 0.003$ meV and $c = 0.2$. Bottom frame: $S(T,\omega) = \lim_{\omega\to 0}\omega\sigma_2(T,\omega) + 2W(T,\omega)/\pi$ in units such that $\lim_{\omega\to\infty} S(T,\omega) = 2$.

IV. APPROXIMATE PARTIAL SUM RULE FOR THE COHERENT PART

In the top frame of Fig. 4 we show our theoretical results for the remaining integrated optical spectral weight under the real part of the conductivity $\sigma_1(T,\omega)$ in the superconducting state up to frequency ω. By definition $W(T,\omega) = \int_{0^+}^{\omega} d\nu\, \sigma_1(T,\nu)$ where the upper limit of the integral is variable. The data is for the very pure sample for which coherent and incoherent contributions are well separated. Results for three temperatures are shown, namely $T = 10$ K (solid line), $T = 15$ K (dashed line), and $T = 20$ K (dotted line) and the variable upper limit ω ranges from zero to 1 meV, i.e. only very low frequencies are sampled, consequently only the coherent quasiparticle contribution to the conductivity (solid curve in the top frame of Fig. 2) is significantly involved since the incoherent contribution is almost negligible in this energy range. Note that already for $\omega \sim 0.4$ meV a well developed plateau is seen in each curve, although its magnitude depends on temperature. $W(T,\omega)$ represents the residual absorption in the microwave region that remains at low temperatures in the superconducting state. It decreases with decreasing temperature as more optical weight is transferred to the condensate. In our calculations this residual absorption has its origin in the

inelastic scattering associated with thermally activated bosons which exist at any finite T and which broadens the quasiparticle contribution. This is in addition to impurity absorption which is also small, when Γ^+ is small. Strictly, at zero temperature only the impurity absorption remains and this goes to zero as Γ^+ goes to zero. We will see later that an extrapolation to zero temperature of the numerical data for $W(T,\omega)$ gives for the cut off $\omega = 1\,\mathrm{meV}$, a value of 0.00023 [in units of $\Omega_p^2/(8\pi)$] which is very small.

In the bottom frame of Fig. 4 we show results for a closely related quantity $S(T,\omega)$ vs ω in units of $\Omega_p^2/(8\pi)$. In the superconducting state, missing spectral weight under the real part of the conductivity when compared to its normal state is found in a delta-function at $\omega = 0$ weighted by the amount in the condensate. In our computer units the full sum rule which applies when $\sigma_1(T,\omega)$ is integrated to infinity and the condensate contribution added, is two. The partial sum up to ω is

$$\begin{aligned} S(T,\omega) &= \lim_{\omega\to 0}\omega\sigma_2(T,\omega) + \frac{2}{\pi}\int_{0^+}^{\omega} d\nu\,\sigma_1(T,\nu) \\ &\equiv \frac{2}{\pi}\int_0^{\omega} d\nu\,\sigma_1(T,\nu), \end{aligned} \tag{9}$$

and is shown for the same three temperatures as in the top frame. Here $\sigma_2(T,\omega)$ is the imaginary part of the conductivity. When multiplied by ω its $\omega \to 0$ limit is proportional to the inverse square of the London penetration depth which, in turn, is proportional to the superfluid density.

For an Eliashberg superconductor the expression for the penetration depth at any temperature T is (in our computer units)

$$\frac{1}{\lambda_L^2(T)} = 8\pi\,T\sum_{\omega_n}\left\langle \frac{\tilde{\Delta}^2_{\mathbf{k}'}(\omega_n)}{[\tilde{\omega}^2(\omega_n)+\tilde{\Delta}^2_{\mathbf{k}'}(\omega_n)]^{3/2}}\right\rangle'. \tag{10}$$

For $T \to 0$ in the constant λ model with no impurities we get

$$\begin{aligned} \frac{1}{\lambda_L^2(T=0)} &= \frac{8\pi}{1+\lambda}\left\langle \int_0^{\infty} d\omega\,\frac{\Delta^2\cos(2\phi')}{[\omega^2+\Delta^2\cos^2(2\phi')]^{3/2}}\right\rangle' \\ &= \frac{1}{\lambda_{cl}^2(0)}\left(\frac{1}{1+\lambda}\right). \end{aligned} \tag{11}$$

where we have restored the units and $\lambda_L^{-2}(T=0)$ is the usual value of the London penetration depth. There are so called strong coupling corrections to Eq. (11) (see Ref. 11) but these are small and, in a first approximation, can be neglected. A physical interpretation of Eq. (11) is that it is only the coherent quasiparticle part of the spectral density (Fig. 1) which significantly participates in the condensation.

Returning to the bottom frame of Fig. 4 we see that at $\omega \sim 0.4\,\mathrm{meV}$ a plateau has been reached in $S(T,\omega)$ vs ω as well and that, relative to what is the case for $W(T,\omega)$ in the top frame, little variation with temperature remains. Nevertheless, the small amount that is seen will have consequences as we will describe later. For now, neglecting this T-dependence, the plateau seen in $S(T,\omega)$ vs ω implies that an approximate partial sum rule will apply to the coherent part of the conductivity by itself, provided the cut off on ω is kept small. This has important implications for the analysis of experiments. While only approximately $1/(1+\lambda)$ of the optical spectral weight is involved in this contribution, this piece behaves like a BCS superconductor. The partial sum rule which applies, when the cut off ω_c is kept below the frequency at which the incoherent part starts to make an important contribution is

$$S(T,\omega_c) = \lim_{\omega\to 0}\omega\sigma_2(T,\omega) + \frac{2}{\pi}\int_{0^+}^{\omega_c} d\nu\,\sigma_1(T,\nu) \simeq \frac{2}{1+\lambda}. \tag{12}$$

in the constant λ approximation of Sec. II. In our full Eliashberg calculations for $T = 10\,\mathrm{K}$ we get ~ 0.71 for Eq. (12) instead of $\sim 2/3$ with $\lambda = 2.01$. It is the existence of the partial sum rule (12) for very pure samples that has allowed Turner *et al.*[14] to analyze their microwave data within a BCS formalism without reference to the mid infrared incoherent contribution. Nevertheless, one has to keep in mind that this partial sum rule involves only $1/(1+\lambda)$ of the whole spectral weight under the $\sigma_1(T,\omega)$ curve with important consequences on the results derived from such an analysis.

For the pure case considered here the cutoff ω_c in (12) is well defined. This is further illustrated in Fig. 5 where we show once more $W(T,\omega)$ (top frame) and $S(T,\omega)$ (bottom frame) but now for an extended frequency range up to 250 meV for the case $T = 10\,\mathrm{K}$ only. We also show, for comparison, additional BCS results and results for a second set of impurity parameters. The solid and dotted curves in both frames are $W(T,\omega)$ and $S(T,\omega)$ for an Eliashberg superconductor with $\Gamma^+ = 0.63\,\mathrm{meV}$, $c = 0$ and $\Gamma^+ = 0.003\,\mathrm{meV}$, $c = 0.2$, respectively. The dashed and dash-dotted curves are for a BCS superconductor with $\Gamma^+ = 0.63\,\mathrm{meV}$, $c = 0$ and $\Gamma^+ = 0.05\,\mathrm{meV}$, $c = 0.2$. We first note that for the purer Eliashberg case (dotted curve) the plateau in both, $W(T,\omega)$ and $S(T,\omega)$ identified in Fig. 4 extends to $\omega \simeq 50\,\mathrm{meV}$. Clearly, any value of frequency between $\omega \simeq 0.4\,\mathrm{meV}$ and 50 meV will do for ω_c in Eq. (12) and a partial sum rule is well defined but for the less pure case (solid curve) a plateau is not as well defined. In both cases, however, the increase beyond the plateau value of ~ 0.7 towards saturation is rather slow and even at $\omega = 250\,\mathrm{meV}$ $S(T,\omega)$ is still well below 2. This feature reflects directly the large energy scale involved in the boson exchange mechanism we have used. This behavior is in sharp contrast to BCS. For the dash-dotted curve $S(T,\omega)$ is already close to two at $\omega \simeq 25\,\mathrm{meV}$ while for the less pure case (dashed curve)

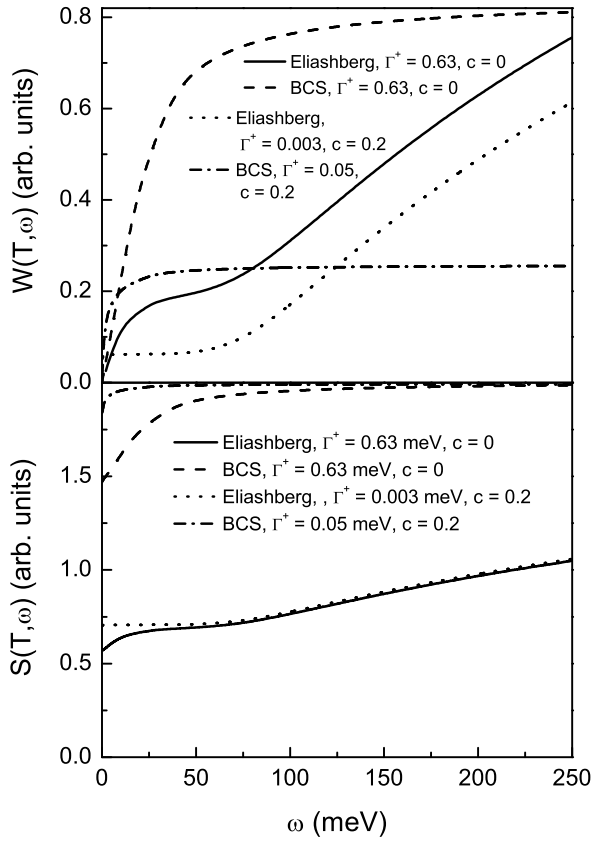

FIG. 5: Top frame: The optical spectral weight $W(T,\omega) = \int_{0^+}^{\omega} d\nu\, \sigma_1(T,\nu)$ as a function of the upper limit ω. Two curves apply to BCS and two correspond to Eliashberg calculations. In one case the unitary limit ($c = 0$) is used with $\Gamma^+ = 0.63\,\mathrm{meV}$ (solid curve for Eliashberg, dashed for BCS). The dotted curve is similar but for $\Gamma^+ = 0.003\,\mathrm{meV}$ and $c = 0.2$ in Eliashberg theory and the dash-dotted is for $\Gamma^+ = 0.05\,\mathrm{meV}$, $c = 0.2$ in BCS. Bottom frame: the same as the top frame but now the sum $S(T,\omega) = \lim_{\omega\to 0}\omega\sigma_2(T,\omega) + (2/\pi)\int_{0^+}^{\omega} d\nu\, \sigma_1(T,\nu)$ is shown. In both frames the temperature $T = 10\,\mathrm{K}$ and the d-wave gap amplitude is the same for Eliashberg and BCS calculations.

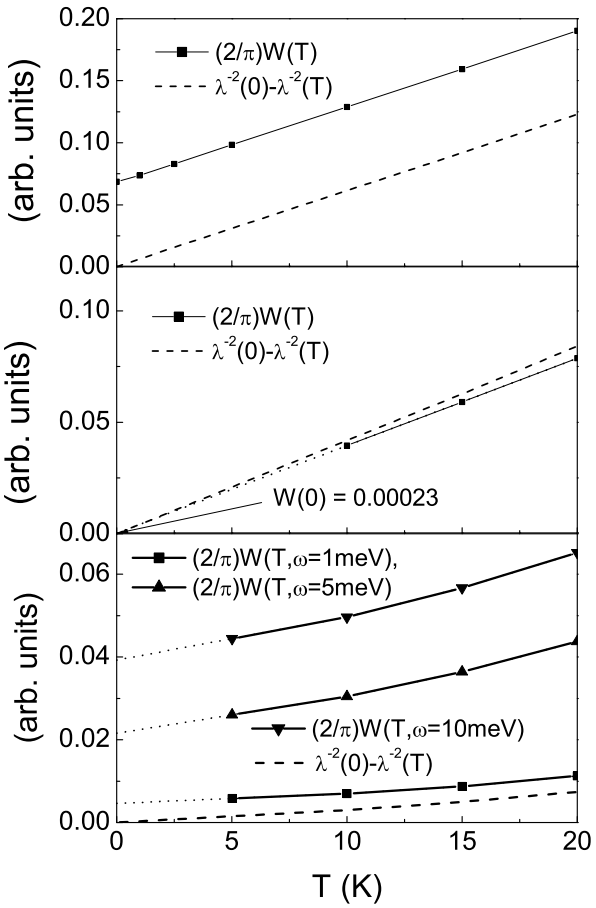

FIG. 6: Top frame: comparison of $(2/\pi)W(T)$ vs T (dotted curve) with $\lambda^{-2}(0) - \lambda^{-2}(T)$ (dashed curve) for a BCS d-wave superconductor with the gap amplitude set at $\Delta = 24\sqrt{2}\,\mathrm{meV}$ and with $\Gamma^+ = 0.1\,\mathrm{meV}$ and $c = 0.3$. The lines are parallel to each other. The superfluid density goes to zero at $T = 0$ while the remaining area under the real part of the conductivity goes to a finite value (residual absorption). Middle frame: same comparison as in the top frame for an Eliashberg superconductor modeled for $YBa_2Cu_3O_{6.99}$, with $\Gamma^+ = 0.003\,\mathrm{meV}$ and $c = 0.2$. The curve for $(2/\pi)W(T)$ extrapolates to a very small value as $T \to 0$ and the two curves are not quite parallel. Bottom frame: same as for the middle frame but with $\Gamma^+ = 0.63\,\mathrm{meV}$ and $c = 0.2$. Three different cut offs in $W(T,\omega)$ are used.

the rise to two is slower and distributed over a larger energy scale of the order $\sim 100\,\mathrm{meV}$. In as much as impurities strongly affect such scale estimates they are not fundamental to the superconductivity itself. If, in our Eliashberg calculations, we look only at the initial rise to its plateau value (~ 0.7), the scales involved are different again, $\sim 1\,\mathrm{meV}$ and $\sim 50\,\mathrm{meV}$ respectively.

V. RELATION BETWEEN RESIDUAL ABSORPTION AND PENETRATION DEPTH

We next turn to the relationship between the temperature dependence of the residual absorption and the penetration depth. This is illustrated in Fig. 6 which has three frames. The top frame presents BCS results and is for comparison with the two other frames which are based on Eliashberg solutions. The central frame has impurity parameters $\Gamma^+ = 0.003\,\mathrm{meV}$ and $c = 0.2$. The bot-

tom frame is for a less pure sample with $\Gamma^+ = 0.63\,\mathrm{meV}$ and $c = 0.2$ and illustrates how impurities change the results. In the top frame, the dashed curve is the difference in superfluid density $\lambda^{-2}(0) - \lambda^{-2}(T)$ as a function of temperature T up to 20 K for a BCS superconductor with gap $\Delta = 24\sqrt{2}\,\mathrm{meV}$, $\Gamma^+ = 0.1\,\mathrm{meV}$, and $c = 0.3$. These parameters were chosen only for the purpose of illustration. Turner *et al.*[14] considered the optical spectral weight concentrated in the microwave region of an ortho-II $YBCO_{6.5}$ sample and the temperature dependence of $W(T)$ that is obtained from consideration of the microwave region only. They found it to extrapolate to a finite value at $T = 0$ (zero temperature residual absorption) while at the same time $W(T)$ parallels the temperature dependence found for the penetration depth. In our solid curve (top frame of Fig. 6 we have integrated $\sigma_1(T,\omega)$ to get $W(T,\omega)$ up to 1 meV and find a curve for $W(T)$ which is parallel to the dashed curve for the penetration depth but indeed does not extrapolate to zero at $T = 0$. Note that in a BCS model for pure samples the ordinary FGT sum rule applies even if only the microwave region is considered and so the solid and dashed curves are parallel. This is no longer the case in Eliashberg theory as shown in the center frame of Fig. 6. There the dashed and solid curves are not quite parallel with the dashed curve showing a slightly steeper slope. Also, the solid curve extrapolates to a finite though very small value at $T = 0$. This is expected since the impurity content in this run is very small. This case corresponds closely to the $YBCO_{6.99}$ sample considered in Fig. 4 of Turner *et al.*[14] The slight difference in slope between solid and dashed curve can be understood in terms of our result for $S(T,\omega_c)$ given in the bottom frame of Fig. 4. We have already noted that at $\omega = 1\,\mathrm{meV}$, the cutoff used in evaluation of $W(T,\omega_c)$ (solid curve, center frame of Fig. 6) there remains a small temperature dependence to the saturated value of $S(T,\omega_c)$. This means that $S(T,\omega_c)$ in this region is slightly smaller at $T = 20\,\mathrm{K}$ (dotted curve in the bottom frame of Fig. 4) than it is at $T = 10\,\mathrm{K}$ (solid curve). This slight deviation from the partial sum rule embodied in our Eq. (12) leads immediately to the difference in slope seen in the center frame of Fig. 6 between $W(T,\omega_c)$ and the penetration depth.

In the bottom frame of Fig. 6 we show results for $\Gamma^+ = 0.63\,\mathrm{meV}$ and $c = 0.2$. In this case the coherent and incoherent contribution to $\sigma_1(T,\omega)$ (see Fig. 3, top frame, dotted curve although this curve is for $c = 0$) are not as well separated as in the pure case and $W(T,\omega)$ vs ω does not show as clear a plateau which would allow the formulation of a partial sum rule on the coherent part alone. Nevertheless, we do note that for $\omega_c = 1\,\mathrm{meV}$, $2W(T,\omega_c)/\pi$ (solid squares) is nearly parallel to the dashed curve for the penetration depth. If, however, ω_c is increased to 5 meV (solid up-triangles), or 10 meV (solid down-triangles) this no longer holds. This result can be traced to the fact that no real temperature and cut off independent plateau is reached in these cases. Thus, there is no partial sum rule which can be applied on $W(T,\omega)$ and an analysis as performed by Turner *et al.*[14] on very high purity samples appears not to be possible. This case may correspond better to the relatively dirtier film data.[15] Note in particular, the residual absorption at zero temperature depends now strongly on the cutoff frequency chosen for the partial sum rule. In our example (bottom frame of Fig. 6) the residual absorption increases almost linearly with increasing cutoff frequency.

We turn next to the zero temperature value of the residual absorption and its impurity dependence. Eq. (10) applies but now we wish to consider impurities so that $\tilde{\omega}_n$ is not simply $\tilde{\omega}_n = \omega_n(1+\lambda)$ in the constant λ model. Instead, we must use

$$\tilde{\omega}(\omega + i0^+) = \omega(1+\lambda) + i\pi\Gamma^+ \frac{\Omega(\omega)}{c^2 + \Omega^2(\omega)}, \qquad (13)$$

which needs to be solved self consistently for $\tilde{\omega}(\omega + i0^+)$. For $\omega = 0$, we can write $\tilde{\omega}(\omega + i0^+) = i\gamma$ with

$$\gamma = \pi\Gamma^+ \frac{\Omega(i\gamma)}{c^2 + \Omega^2(i\gamma)} \qquad (14)$$

and $\Omega(i\gamma)$ is given by Eq. (3). Evaluating $\Omega(i\gamma)$ gives

$$\gamma = \pi\Gamma^+ \frac{\frac{2\gamma}{\pi\Delta(1+\lambda)} \ln\left(\frac{4\Delta(1+\lambda)}{\gamma}\right)}{c^2 + \left(\frac{2\gamma}{\pi\Delta(1+\lambda)}\right)^2 \ln^2\left(\frac{4\Delta(1+\lambda)}{\gamma}\right)}. \qquad (15)$$

This transcendental equation for γ, the zero frequency scattering rate at zero frequency, is to be solved numerically for any value of c. Results can be found in Refs. 36 and 38 for the case $\lambda = 0$. What is found is that γ/c increases with Γ^+ and, for a given value of Γ^+ decreases rapidly with c. At $c = 0$ we get the approximate, but very useful relation

$$\gamma = 0.63\sqrt{\pi\Gamma^+\Delta(1+\lambda)}. \qquad (16)$$

Note, this is the same expression as in Hirschfeld and Goldenfeld[40] except that it contains an additional factor of $(1+\lambda)$. In terms of γ we can get an approximate expression for the zero temperature London penetration depth including impurities. Returning to Eq. (10) we need to replace $\tilde{\omega}_n$ by $\omega_n(1+\lambda) + \gamma$ to get[38]

$$\frac{1}{\lambda_L^2(0)} = 8\pi\frac{1}{1+\lambda}\int_0^{2\pi}d\phi\int_0^{\infty}d\omega\,\frac{\Delta^2\cos^2(2\phi)}{\left[\left(\omega+\frac{\gamma}{1+\lambda}\right)^2+\Delta^2\cos^2(2\phi)\right]^{3/2}} \quad (17)$$

$$\simeq \frac{1}{\lambda_{cl}^2(0)}\left\{1-\frac{2}{\pi}K\left[\frac{i}{\gamma}\Delta(1+\lambda)\right]\right\}, \quad (18)$$

where $K(x)$ is the elliptic integral of the first kind. The approximation made to get the last equality, Eq. (18), is not very accurate but has the the important advantage that it is analytic and simple. It gives

$$\lambda_L^{-2}(0) \simeq \lambda_{cl}^{-2}(0)\left[1-\frac{2\gamma(1+\lambda)}{\pi\Delta}\ln\left(\frac{4\Delta(1+\lambda)}{\gamma}\right)\right]. \quad (19)$$

In a BCS model ($\lambda = 0$) this gives in the limits $T \to 0$ and $\omega \to \infty$

$$W(T=0,\omega\to\infty)\equiv W(0) = \int_{0^+}^{\infty}d\omega\,\sigma_1(0,\omega) = \frac{\gamma}{\Delta}\ln\left(\frac{4\Delta}{\gamma}\right). \quad (20)$$

Exact numerical results for $W(0)$ based on Eq. (17) with $\lambda = 0$ are compared with those based on Eq. (20) in the top frame of Fig. 7. We see that Eq. (20) is qualitatively but not quantitatively correct. In the bottom frame we show the corresponding values of $\gamma(c)$ vs c for the convenience of the reader. It is clear that the residual absorption due to the coherent part of the charge carrier spectral density does depend significantly on impurity content. In a real superconductor we have additional absorption at $T = 0$ coming from the incoherent, boson assisted background which enters when ω in the upper limit of the defining integral for $W(T,\omega)$ is made to span energies in the infrared region of the spectrum.

VI. MISSING AREA

The FGT sum rule implies that the missing optical spectral weight under the real part of the conductivity in the superconducting state appears as a delta function contribution at the origin proportional to the superfluid density. It depends on temperature and on impurity content. Increasing T and/or Γ^+ decreases the superfluid density. In the top frame of Fig. 8 we show our results for the remaining integrated optical spectral weight $W(T,\omega)$ as a function of ω up to 250 meV for a sample with $\Gamma^+ = 0.63$ meV and $c = 0$. We have done similar calculations for a clean sample but there is no qualitative difference. The solid curve is for the superconducting state at $T = 10$ K and is to be compared with the dotted curve which is for the normal state at the same temperature. We see a great deal of missing spectral weight between these two curves with $W_N(T,\omega)$ rising much faster at small ω than $W_S(T,\omega)$ and it is rising to a much higher value. The difference $W_N(\omega,T=10\,\mathrm{K}) - W_S(\omega,T=10\,\mathrm{K})$ (dashed curve) is the amount of optical spectral weight between $(0^+,\omega)$ that has been transferred to the superfluid condensate. As we see, the dashed curve rapidly grows within a few meV to a value close (but not quite) to the asymptotic value it assumes at $\omega = 250$ meV. After this the remaining variation is small but there is a shallow minimum around 30 meV with a corresponding broad and slight peak around 100 meV which is followed by a small gradual decrease still seen at 250 meV. These features can be understood in detail when the frequency dependence of $\sigma_1(T,\omega)$ is considered. The relevant curves to be compared are the dotted (normal) and solid (superconducting) in the bottom frame of Fig. 8. Both are at 10 K. The curves cross at 3 places on the frequency axis. Above the first crossing at $\omega_1 \approx 8$ meV the difference in the integrated area decreases till $\omega_2 \approx 32$ meV at which it begins to increase. Finally, at the third crossing $\omega_3 \approx 130$ meV it begins to decrease again towards its value at 250 meV. These features are the direct result of the shift in incoherent background towards higher energies due to the opening up of the superconducting gap. The area between the dotted and solid lines that falls between ω_2 and ω_3 is made up slowly at higher frequencies. This feature would not be part of BCS theory in which case the energy scale for the optical weight which significantly participates in the condensate is set as a few times the gap Δ[41] and the saturated value is reached from below rather than from above. In our theory the existence of the incoherent background effectively increases this scale to much higher energies, the scale set by the bosons involved, although the amount of spectral weight involved is very small.[42,43] We note that at $\omega = 250$ meV the missing area curves $W_N(T=10\,\mathrm{K},\omega) - W_S(T=10\,\mathrm{K},\omega)$ and $W_N(T=95\,\mathrm{K},\omega) - W_S(T=10\,\mathrm{K},\omega)$ of the top frame of Fig. 8 are still about 2.5% higher than the value indicated for the penetration depth (thin dash-double dotted line) which is obtained directly from the imaginary part of the optical conductivity.

In an actual experiment it is not possible to access the normal state at low temperatures so that $W_N(\omega,T=10\,\mathrm{K})$ cannot be used to compute the difference with $W_S(\omega,T=10\,\mathrm{K})$. Usually $W_N(\omega,T=95\,\mathrm{K})$ is used

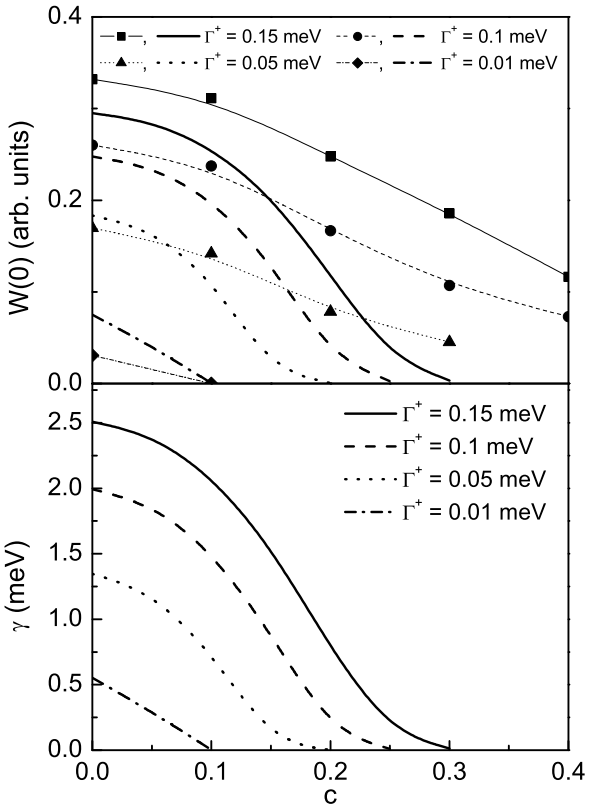

FIG. 7: Top frame: the $T \to 0$ limit of the remaining optical spectral weight $W(0) = \int_{0^+}^{\infty} d\omega\, \sigma_1(T=0,\omega)$ as a function of the impurity potential strength c for various values of Γ^+. The heavy continuous curves are the approximation $W(0) \simeq (\gamma/\Delta)\ln(4\Delta/\gamma)$ while the light curves with solid squares ($\Gamma^+ = 0.15\,\mathrm{meV}$), solid circles ($\Gamma^+ = 0.1\,\mathrm{meV}$), solid triangles ($\Gamma^+ = 0.05\,\mathrm{meV}$), and solid diamonds ($\Gamma^+ = 0.01\,\mathrm{meV}$) are exact results. The bottom frame gives the zero frequency value of the effective scattering in the superconducting state, $\gamma(c)$ as a function of c.

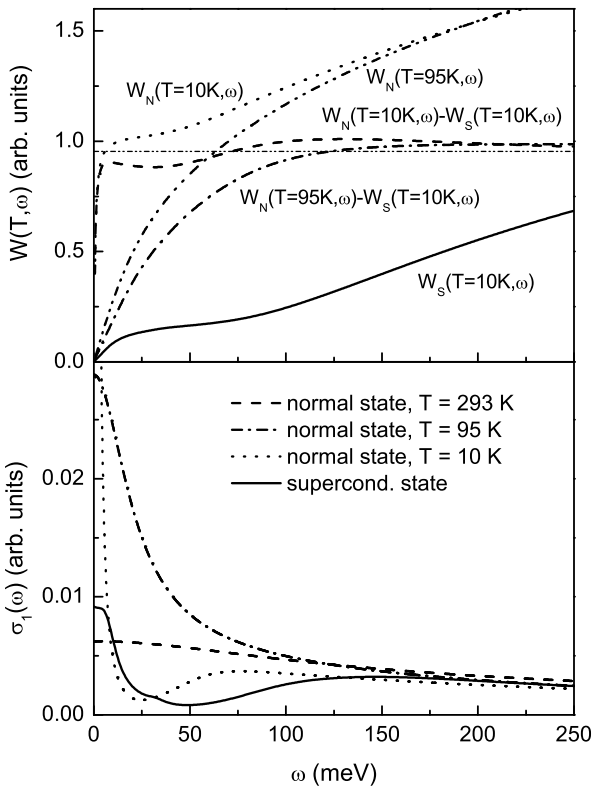

FIG. 8: Top frame: optical spectral weight $W(\omega,T) = \int_{0^+}^{\omega} d\nu\, \sigma_1(\nu)$ for various cases as a function of ω. The dotted (dash-double dotted) curve is for the normal state at $T = 10\,\mathrm{K}$ ($T = 95\,\mathrm{K}$), the solid curve for the superconducting state at $T = 10\,\mathrm{K}$. The dashed (dash-dotted) curve is the difference curves between superconducting and normal state ($\tilde{\Delta}(\omega) = 0$ in the Eliashberg equations) at $T = 10\,\mathrm{K}$ ($T = 95\,\mathrm{K}$). The approach of the difference in area to its saturated large ω value depends significantly on the temperature used for the subtracted normal state. The thin dash-double dotted horizontal line is the value of the penetration depth. Bottom frame: it shows the real part of the conductivity for the normal state at $T = 293\,\mathrm{K}$ (dashed curve), $T = 95\,\mathrm{K}$ (dash-dotted curve), $T = 10\,\mathrm{K}$ (dotted curve), and for the superconducting state a $T = 10\,\mathrm{K}$ (solid curve). All curves are for $YBCO_{6.95}$ with the impurity parameters set to $\Gamma^+ = 0.63\,\mathrm{meV}$ and $c = 0$.

instead. This is shown as the dashed-double dotted curve in the top frame of Fig. 8 which is seen to merge with the dotted curve only at large values of ω. Because in our theoretical work, the inelastic scattering at $T = T_c$ is large with a scattering rate of the order $2T_c$ or so, the corresponding optical spectral weight in $\sigma_1(T,\omega)$ is shifted to higher energies. Consequently, $W_N(\omega, T = T_c)$ rises much more slowly out of $\omega = 0$ than does $W_N(\omega, T = 10\,\mathrm{K})$ and the difference curve $W_N(\omega, T = 95\,\mathrm{K}) - W_S(\omega, T = 10\,\mathrm{K})$ (dash-dotted curve) reflects this. It merges with the dashed curve only for $\omega \gtrsim 200\,\mathrm{meV}$. Thus, making use of $W_N(\omega, T = T_c)$ rather than $W_N(\omega, T = 10\,\mathrm{K})$ makes a considerable difference in the estimate of the ω dependence of the missing area. None of the structure seen in the dashed curve remains in the dash-dotted curve and much information on separate coherent and incoherent contributions is lost, although the curve still approaches its $\omega \to \infty$ limiting value from above. From this point of view, it is the dashed curve which is fundamental but it is not directly available in experiments. If an even higher temperature had been used for the normal state, say around room temperature, the frequency at which the difference $W_N(\omega) - W_S(\omega)$ would agree with the penetration depth is pushed to very high energies well beyond the 250 meV range shown in the top frame of Fig. 8. The reason for this is clear when the bottom frame of this same figure is considered.

What is shown is the real part of the conductivity for four cases: the normal state at $T = 293\,\mathrm{K}$ (dashed curve), at $T = 95\,\mathrm{K}$ (dash-dotted curve), and at $T = 10\,\mathrm{K}$ (dotted curve). Increasing the normal state temperature shifts a lot of spectral weight to higher energies and can even make the difference $W_N - W_S$ negative for small ω.

We stress again that individual $W(T,\omega)$ curves show no saturation as a function of ω in the range shown. This is characteristic of the high T_c oxides and resides in the fact that $I^2\chi(\omega)$, the electron-boson exchange spectral density, extends to very high energies. This is fundamental to an understanding of the optical properties in these materials and is very different from the electron-phonon case. In that instance there is a maximum phonon energy ω_D never larger than about 100 meV and hence the curve for $W(T,\omega)$ would reach saturation at a much smaller energy than in our work. This observation provides strong evidence against solely a phonon mechanism for superconductivity in the oxides.

To aid this discussion we added Fig. 9 which, in its top frame, shows the experimental data for the real part of the optical conductivity, $\sigma_1(T,\omega)$ reported by Tu *et al.*[33] in an optimally doped $Bi_2Sr_2Ca\,Cu_2O_{8+\delta}$ (Bi2212) single crystal for three temperatures, namely, $T = 6$, 100, 295 K. The experimental data has been augmented by theoretical data[5] in the frequency region $0 < \omega \leq 12.4\,\mathrm{meV}$ derived from best fits to experiment. This graph is to be compared with the bottom frame of Fig. 8. The bottom frame of Fig. 9 presents the corresponding optical spectral weight $W(\omega,T)$ calculated from the experimental $\sigma_1(\omega,T)$ data. The results follow closely similar theoretical curves presented in the top frame of Fig. 8. In particular, $W_S(\omega, T = 6\,\mathrm{K})$ does not develop a well defined plateau around 50 meV as we found it for optimally doped $YBCO_{6.95}$ single crystals [solid line in the top frame of Fig. 8, labeled $W_S(T = 10\,\mathrm{K},\omega)$]. Finally, the differences $W_N(\omega, T = 100\,\mathrm{K}) - W_S(\omega, T = 6\,\mathrm{K})$ (solid line) and $W_N(\omega, T = 295\,\mathrm{K}) - W_S(\omega, T = 6\,\mathrm{K})$ (dash-double dotted line) are shown in this graph. We also included the theoretical value for $(\pi/2)\lim_{\omega\to 0}\omega\sigma_2(\omega, T = 6\,\mathrm{K})$ as a thin, solid horizontal line found from a fit to experimental data. The first difference is still far away from this limit but approaches it from above, as expected from our previous discussion, while the second approaches this limit from below. This analysis of experimental data supports our theoretical results in a rather impressive way.

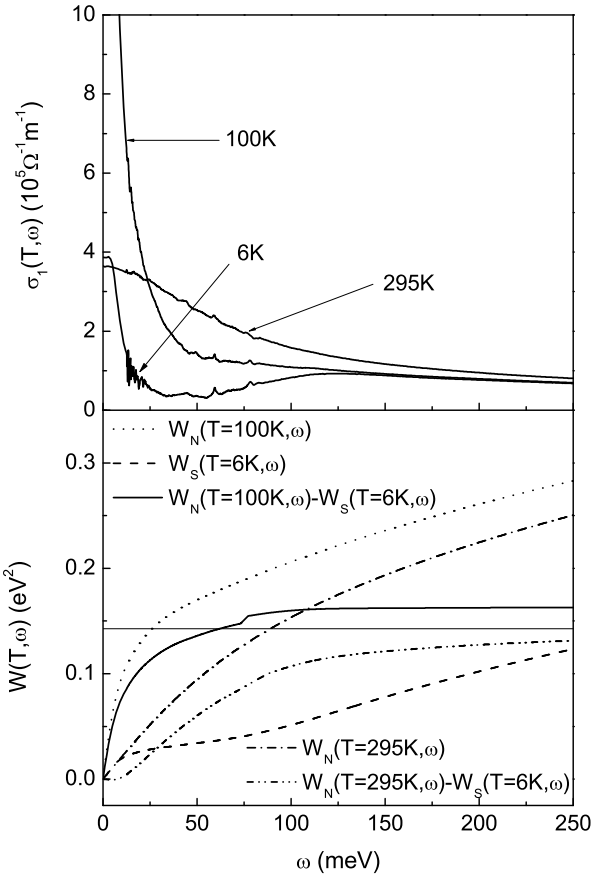

FIG. 9: Top frame: Experimental data for the real part of the optical conductivity, $\sigma_1(\omega)$ vs ω and various temperatures for an optimally doped Bi2212 single crystal as it was reported by Tu *et al.*[33] The data has been augmented by theoretical data[5] in the energy range $0 < \omega \leq 12.\,\mathrm{meV}$. Bottom frame: Optical spectral weight $W(\omega,T) = \int_{0^+}^{\omega} d\nu\,\sigma_1(\nu,T)$ vs ω as calculated from the experimental data shown in the top frame of this figure. The dashed line is for $T = 6\,\mathrm{K}$ (superconducting state), the dotted line for $T = 100\,\mathrm{K}$, and the dash-dotted line for $T = 295\,\mathrm{K}$. Presented are also the differences $W_N(\omega, T = 295\,\mathrm{K})$-$W_S(\omega, T = 6\,\mathrm{K})$ (dash-double dotted line) and $W_N(\omega, T = 100\,\mathrm{K})$-$W_S(\omega, T = 6\,\mathrm{K})$ (solid line). The thin, solid horizontal line represents the theoretical value $(\pi/2)\lim_{\omega\to 0}\omega\sigma_2(\omega, T = 6\,\mathrm{K})$.

VII. CONCLUSIONS

In a pure BCS superconductor at zero temperature with no impurities the entire optical spectral weight under the real part of the conductivity will vanish as it is all transferred to the superfluid density which contributes a δ-function at $\omega = 0$ to the real part of $\sigma(\omega)$. When impurities are present the superfluid density at $T = 0$ is reduced from its clean limit value and some spectral weight remains under $\sigma_1(\omega)$ which implies some absorption even at zero temperature. The situation is quite different for a superconductor which shows a pronounced incoherent background scattering which can be modeled reasonably well in Eliashberg theory be it *s*- or *d*-wave. In both cases it is mainly the coherent part of the electron spectral density which contributes to the condensate. The electron spectral function still has a δ-function part broadened by the interactions at any finite energy away from the Fermi energy but the amount of weight under this part is $1/(1+\lambda)$, where λ is the mass enhancement parameter for the electron-boson exchange interaction. The remain-

ing spectral weight $\lambda/(1+\lambda)$ is to be found in incoherent, boson assisted tails. Another way of putting this is that at zero temperature in a pure system the superfluid density is related to the renormalized plasma frequency with m^* replacing the bare electron mass ($m^*/m = 1+\lambda$) in contrast to the total plasma frequency which involves the bare mass m. The incoherent, boson assisted tails in $\sigma_1(T,\omega)$ do not contribute much to the condensate and in fact remain pretty well unaffected in shape and optical weight by the transition to the superconducting state but they are shifted upwards due to the opening up of the superconducting gap. This shift implies that when one considers the missing optical spectral weight under the conductivity which enters the condensate, the energy scale for this readjustment is not set by the gap scale but rather by the scale of the maximum exchanged boson energy. Also it is expected that the value of the penetration depth which corresponds to the saturated value of the missing area is approached from above when the conductivity is integrated to high energies.

Acknowledgment

Research supported by the Natural Sciences and Engineering Research Council of Canada (NSERC) and by the Canadian Institute for Advanced Research (CIAR). J.P.C. thanks D.M. Broun for discussions. The authors are grateful to Drs. C.C. Homes and J.J. Tu for providing their original experimental data for analysis.

* Electronic address: schachinger@itp.tu-graz.ac.at; URL: `www.itp.tu-graz.ac.at/~ewald`

[1] F. Marsiglio and J.P. Carbotte, Aust. J. Phys. **50**, 975 (1997), and **50**, 1011 (1997).
[2] R.A. Ferrell and R.E. Glover, Phys. Rev. **109**, 1398 (1958).
[3] M. Tinkham and R.B. Ferrell, Phys. Rev. Lett. **2**, 331 (1959).
[4] H.J.A. Molegraaf, C. Presura, D. van der Marel, P.H. Kes, and M. Li, Science **295**, 2239 (2002).
[5] E. Schachinger and J.P. Carbotte, J. Phys. Studies (L'viv, Ukraine) **7**, 209 (2003); E. Schachinger and J.P. Carbotte, in: *Models and Methods of High-TC Superconductivity: some Frontal Aspects, Vol. II*, ed.: J.K. Srivastava and S.M. Rao, Nova Science, Hauppauge NY (2003), pp. 73.
[6] S.M. Quinlan, P.J. Hirschfeld, and D.J. Scalapino, Phys. Rev. B **53**, 8575 (1996).
[7] P.J. Hirschfeld, S.M. Quinlan, and D.J. Scalapino, Phys. Rev. B **55**, 12 742 (1997).
[8] S.M. Quinlan, D.J. Scalapino,and N. Bulut, Phys. Rev. B **49**, 1470 (1994).
[9] P.J. Hirschfeld, W.O. Putikka, and D.J. Scalapino, Phys. Rev. B **50**, 10250 (1994).
[10] F. Marsiglio and J.P. Carbotte, in Handbook on Superconductivity: Conventional and Unconventional, eds. K.H. Bennemann and J.B. Ketterson (Springer, Berlin, 2003), pp. 233-345.
[11] J.P. Carbotte, Rev. Mod. Phys. **62**, 1027 (1990).
[12] D.B. Tanner, H.L. Liu *et al.*, Physica B **244**, 1 (1998).
[13] H.L. Liu, N.A. Quijada, *et al.*, J. Phys.: Condens. Matter **11**, 239 (1999).
[14] P.J. Turner, R. Harris, S. Kamal, M.E. Hayden, D.M. Broun, D.C. Morgan, A. Hosseini, P. Dosanjh, G. Mullins, J.S. Preston, R. Liang, D.A. Bonn, and W.N. Hardy, Phys. Rev. Lett. **90**, 237005 (2003).
[15] J. Corson, J. Orenstein, Seongshik Oh, J. O'Donnell, and J.N. Eckstein, Phys. Rev. Lett. **85**, 2569 (2000).
[16] E. Schachinger and J.P. Carbotte, Phys. Rev. B **67**, 134509 (2003).
[17] G. Grimvall, The Electron-Phonon Interaction in Metals, (North-Holland, New York, 1981).
[18] A. Millis, H. Monien, and D. Pines, Phys. Rev. B **42**, 167 (1990).
[19] P. Monthoux and D. Pines, Phys. Rev. B **47**, 6069 (1993); Phys. Rev. B **49**, 4261 (1994); Phys. Rev. B **50**, 16015 (1994).
[20] J.P. Carbotte, E. Schachinger, and D.N. Basov, Nature (London) **401**, 354 (1999).
[21] E. Schachinger and J.P. Carbotte, Phys. Rev. B **62**, 9054 (2000).
[22] E. Schachinger, J.P. Carbotte, and D.N. Basov, Europhys. Lett. **54**, 380 (2001).
[23] E. Schachinger and J.P. Carbotte, Physica C **364**, 13 (2001).
[24] C.M. Varma, Int. J. Mod. Phys. **3**, 2083 (1989).
[25] P.B. Littlewood, C.M. Varma, S. Schmitt-Rink, and E. Abrahams, Phys. Rev. B **39**, 12371 (1989).
[26] C.M. Varma, P.B. Littlewood, S. Schmitt-Rink, E. Abrahams, and A.E. Ruckenstein, Phys. Rev. Lett. **63**, 1996 (1989); *ibid.* **64**, 497 (1990).
[27] W.L. McMillan and J.M. Rowell, Phys. Rev. Lett. **19**, 108 (1965).
[28] W.L. McMillan and J.M. Rowell, in Superconductivity, ed. R.D. Parks (Marcel Dekker Inc., New York, 1969), p. 561.
[29] F. Marsiglio, T. Startseva, and J.P. Carbotte, Phys. Lett. A **245**, 172 (1998).
[30] Ph. Bourges, Y. Sidis, H.F. Fong, B. Keimer, L.P. Regnault, J. Bossy, A.S. Ivanov, D.L. Lilius, and I.A. Aksay, in High Temperature Superconductivity, eds. S.E. Barnes, *et al.*, CP483 (American Institute of Physics, Amsterdam, 1999), p. 207.
[31] A.V. Puchkov, D.N. Basov, and T. Timusk, J. Phys.: Condens. Matter **8**, 10049 (1996).
[32] C.C. Homes, D.A. Bonn, R. Liang, W.N. Hardy, D.N. Basov, T. Timusk, and B.P. Clayman, Phys. Rev. B **60**, 9782 (1999).
[33] J.J. Tu, C.C. Homes, G.D. Gu, D.N. Basov, and M. Strongin, Phys. Rev. B **66**, 144514 (2002).
[34] S. Sorella, G.B. Martins, F. Becca, C. Gazza, L. Capriotti, A. Parola, and E. Dagotto, Phys. Rev. Lett. **88**, 117002 (2002).
[35] A. Hosseini, R. Harris, S. Kamal, P. Dosanjh, J. Preston, R. Liang, W.N. Hardy, and D.A. Bonn, Phys. Rev. B **60**, 1349 (1999).
[36] E. Schachinger and J.P. Carbotte, Phys. Rev. B **64**, 094501

(2001).
[37] P.A. Lee, Phys. Lett. **71**, 1887 (1993).
[38] E. Schachinger and J.P. Carbotte, Phys. Rev. B **65**, 064514 (2002).
[39] I. Schürrer, E. Schachinger, and J.P. Carbotte, Physica C **303**, 287 (1998); J. Low Temp. Phys. **115**, 251 (1999).
[40] P.J. Hirschfeld and N. Goldenfeld, Phys. Rev. B **48**, 4219 (1993).
[41] A.E. Karakozov, E.G. Maksimov, and O.V. Dolgov, Solid State Commun. **124**, 119 (2002).
[42] C.C. Homes, S.V. Dordevis, D.A. Bonn, R. Liang, and W.N. Hardy, cond-mat/0303506 (unpublished).
[43] A.F. Santander-Syro, R.P.M.S. Lobo, N. Bontemps, Z. Konstantinovic, Z.Z. Li, and H. Raffy, Europhys. Lett. **62**, 568 (2003).